*Seminarios de la SEM, Vol. 4, 66-102*

# Computer simulations of surfaces and interfaces: a case study of the hydration and dissolution of α-quartz $SiO_2$

***Nora H. de Leeuw***

Department of Chemistry, University College London, 20 Gordon Street, London WC1H 0AJ, UK

*The aim of this chapter is to describe two approaches to modelling the structures and energetics of surface and interface processes of oxide minerals, using both classical atomistic simulations and electronic structure calculations. We will illustrate the application of these techniques by describing some of our recent work using electronic structure calculations to elucidate the structures and stabilities as well as the hydration and dissolution behaviour a selection of α-quartz surfaces.*

## 1. Introduction

Understanding extended defects such as surfaces and interfaces is important as they control the physical and chemical properties of minerals and ceramics including electronic and ionic conduction, diffusion, creep, crystal growth, corrosion, reactivity and catalysis (Duffy, 1986; Sakaguchi et al., 1992). Experiments that probe the structure and stability at the atomic level are often difficult and hence computer simulation can been used as a complementary tool to gain understanding of the structure and properties of such defects (Duffy, 1986; Tasker, 1987; Puls et al., 1977). The classical atomistic simulation of the surfaces of ionic solids was pioneered by the work of Tasker (1979) and Mackrodt and Stewart (1979). Much of the early work was confined to modelling planar surfaces of the cubic rocksalt oxides MgO, CaO and NiO (Colbourn et al., 1983; Tasker and Duffy, 1984; Tasker et al., 1985), later extended to more complicated materials such as $Cr_2O_3$ (Lawrence et al., 1987), $Al_2O_3$ (Mackrodt, 1989) and $Fe_3O_4$ (Davies et al., 1994). Further complexity has been afforded by the development of models for oxy-anions such as $SO_4^{2-}$, $CO_3^{2-}$ and $PO_4^{3-}$ which has led to surface simulations of, for example, $CaCO_3$ minerals (de Leeuw and Parker, 1997, 2000), $Na_2SO_4$ polymorphs (Cooper and de Leeuw, 2006) and $Ca_{10}(PO_4)_6(F,OH)_2$ (Rabone and de Leeuw, 2006; Filgueiras et al., 2006).

One of the major research areas in computational surface science is the surface-water interface, as the growing interest in crystal growth and dissolution processes means that we can no longer meaningfully model surfaces in a vacuum but have to take into account the rôle of water in these processes (e.g. de Leeuw and Parker, 1997, 1998; de Leeuw et al., 1999; Mkhonto and de Leeuw, 2002; Cooper and de Leeuw, 2003, 2004). More recently, the adsorption of organic matter at mineral surfaces is also beginning to be addressed (Filgueiras et al., 2006; Cooper and de Leeuw, 2004; de Leeuw and Cooper, 2004; Mkhonto et al., 2006) as organic surfactants are well known contaminants in soils, flotation reagents for mineral separation, and crystal growth enhancers/inhibitors.

In addition to these classical surface modelling methods, the increase in computer power and memory over the last few years has made it possible to model surfaces using electronic structure calculations, usually employing methods based on the Density Functional Theory. For example, Manassidis and Gillan (1994) investigated surfaces of α-alumina while the work of Schroer et al. (1994) concentrated on ZnO and CdS surfaces. Since then, a wide range of materials has been studied, from metals such as iridium (Barrett et al., 1991) and copper (Klepeis and Terminello, 1996) to semiconductors such as $ErSi_{1.7}$ (Stauffer et al., 1995) and InAs (Swanston et al., 1994) as well as oxides like MgO (Kantorovich et al., 1995), $SnO_2$ and $TiO_2$ (Goniakowski et al., 1996; Purton et al., 1995). Another aspect of surfaces which has been modelled extensively during the last few years is adsorption of various small molecules on metals, such as CO on palladium (Mijoule and Bouteiller, 1991) and nickel (Gorling et al., 1993; Burghgraef et al., 1993) and $Cl_2$ on silver (de Leeuw et al., 2004), as well as adsorption at oxide surfaces, including CO and water on $TiO_2$ (Pacchioni et al., 1996; Goniakowski and Gillan, 1996), $NH_3$ on MgO (Pugh and Gillan, 1994) and $O_2$ on $FeSbO_4$ (Grau-Crespo et al., 2007). Apart from these static calculations, electronic structure molecular dynamics simulations have also been performed by various groups, as for instance the dissociative chemisorption of $Cl_2$ on silicon (Payne et al., 1993; Stich et al., 1994). However, these methods are, at present, still restricted in the number of atoms that can be treated and hence we find that the application of a combination of accurate electronic structure techniques, together with more approximate classical simulations for larger systems, is an efficient approach to model detailed surface structures and complex interfaces. If care is taken when choosing the basis sets and functionals of electronic structure calculations and the parameters for the interatomic potential simulations, the two types of techniques often show excellent quantitative agreement as to structures and energies of the systems under investigation (de Leeuw and Cooper; 2003), and hence can be used as complementary methods for the study of a range of mineral properties.

## 2. Simulating Surfaces and Interfaces

There are two approaches to the computer modelling of solid surfaces, employing either a two-dimensional or a three-dimensional simulation cell. In both cases, periodic boundary conditions are usually employed to limit the computer time required to model a system of realistic size. Periodic boundary conditions enable a finite number of particles to generate realistic behaviour by mimicking an infinite system in such a way that when a particle leaves the simulation box an image rejoins the box on the opposite side. The box of particles is thus surrounded by images of itself, producing an infinite repeat of the simulation cell in either two or three dimensions. Periodic boundary conditions are therefore very effective in modelling crystalline materials and it is also adequate for liquids or amorphous materials provided that any long-range properties are not considered.

### *2.1. Two-dimensional Periodicity*

In the computer code METADISE (Watson et al., 1996), which is designed to model surfaces and interfaces as well as dislocations, the crystal is considered to consist of a series of (charged) planes parallel to the surface and periodic in two dimensions. The crystal is then divided into two blocks, each of which is divided into two regions, region I and region II (Figure 1a). The ions in region I are allowed to relax explicitly while those in region II are held fixed at their bulk equilibrium positions, although the two region IIs are allowed to move relative to each other. It is necessary to include region II to ensure that the potential of an ion at the bottom of region I is modelled correctly (Tasker, 1979). A surface is created when block II is removed with the top of region I as the free surface (Figure 1b). Interfaces such as stacking faults and grain boundaries can be studied by fitting two surface blocks together in different orientations.

The energy of the crystal is made up of two parts:

$$U_{latt} = U_1 + U_2 \tag{1}$$

where $U_1$ and $U_2$ are the energies of the combined ions in region I and region II respectively. The energy of region I is given as follows:

$$U_1 = \sum_{\substack{i\in I \\ j\in I}} \sum_{1} \Psi_{ij}\left(\left|r_{ij} - r_1\right|\right) + \frac{1}{2} \sum_{\substack{i\in I \\ j\in II}} \sum_{1} \Psi_{ij}\left(\left|r_{ij} - r_1\right|\right) \tag{2}$$

where $\Psi_{ij}$ is some suitable pair potential. The first term includes interactions between the ions in region I only and the second term describes the interactions between the ions in region I and those in region II, which is referred to as the boundary interaction

energy. The energy of region II consists only of this boundary interaction energy because the ions are kept fixed and hence the interaction between the ions in region II itself is unchanged and can therefore be ignored. The energy contribution is thus as follows:

$$U_2 = \frac{1}{2}\sum_{\substack{i\in I \\ j\in II}} \Psi_{ij}\left(\left|r_{ij} - r_1\right|\right) \qquad (3)$$

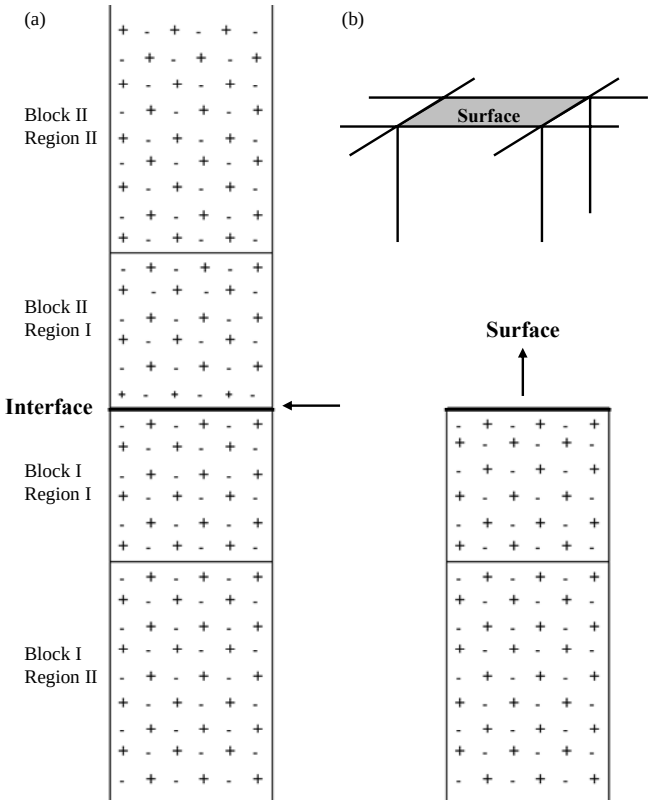


***Figure 1****. The two region approach used in METADISE. (a) the complete crystal and (b) half a crystal, exposing a surface, periodic in two dimensions.*

### *2.1.1. Solid/solid Interfaces*

In addition to modelling either the perfect bulk crystal or a mineral surface with the use of METADISE, it is also possible to use the same procedure to model solid/solid interfaces, either grain boundaries within a single mineral or interfaces between two different materials. The interfacial systems that we can create are either tilt or twist

boundaries, as shown in Figure 2. From the calculations we obtain both a quantitative measure of the stability of the interface, as well as the energy of adhesion of the two solids across the interface.

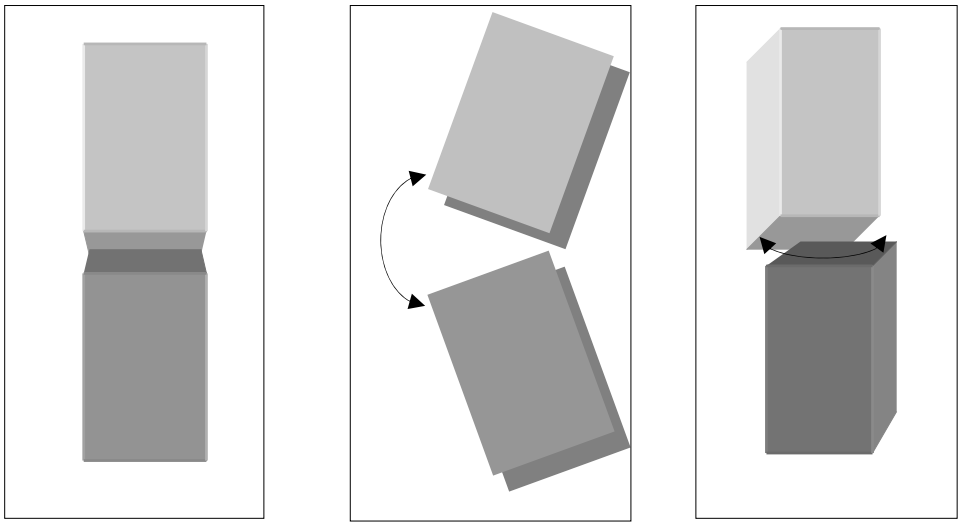

***Figure 2****. Building solid/solid interfaces, (a) perfect alignment of the two systems, leading to the bulk if the two blocks are the same mineral (b) a tilt interface and (c) a twist interface.*

This method to produce solid/solid interfaces has been applied to a range of tilt grain boundaries of the mineral forsterite $Mg_2SiO_4$, the magnesium end-member of the olivine group of minerals (de Leeuw et al., 2000a). The forsterite {010} surface is found to be the dominant surface in the crystal morphology, both experimentally and computationally (Deer et al., 1992; de Leeuw et al., 2000b) and we have created a series of {010} tilt grain boundaries in two orthogonal surface directions with an increasing area of the {010} terrace. Two of the structures are shown in Figure 3. It was found that the formation energy of the grain boundaries with respect to the bulk material is determined both by the stability of the interface on the one hand and the stability of the surfaces making up the mirror grain boundaries on the one hand, where an increasing {010} terrace leads to an increasing surface stability (de Leeuw et al., 2000a).

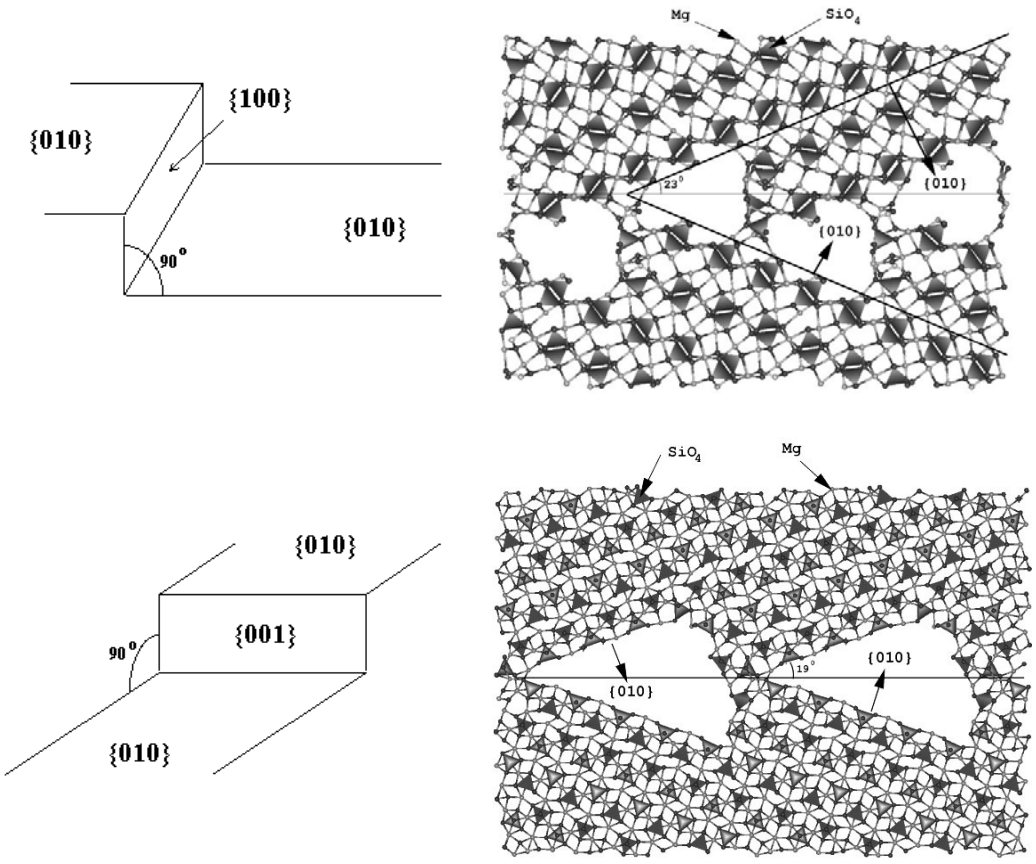


***Figure 3****. Geometry optimized structures of forsterite (010) mirror boundaries with {010} terraces of 1.4 nm$^2$, with (a){100} step wall showing two round channels per terrace at the interface and (b) {001} step wall showing one triangular channel per terrace.*

### *2.2. Three-dimensional Periodicity*

When we use three-dimensional periodic boundary conditions, as for example in our electronic structure calculations of the α-quartz (0001) surfaces described below, the approach for modelling a surface is first to simulate the bulk crystal, which has to be orientated in such a way that two of the three lattice vectors lie in the plane of the surface that we are investigating. A simulation of the bulk crystal is run to obtain the relaxed lattice constants and crystal structure. The surface is then created by expanding the lattice vector in the stacking direction (this is the third lattice vector which is the only one to have a component perpendicular to the surface), which creates a slab of material with two surfaces and a void between itself and its images in the stacking

direction (Figure 4). It is important that the void is big enough so that no interactions occur between one surface of the slab and its image across the void. Care must also be taken that the slab itself contains enough layers of material to behave as bulk crystal in the middle of the slab and to prevent ions at the surface experiencing interactions with the other face through the slab itself. Once created, the surface structures and energies can be calculated keeping the lattice vectors of this system of slab and void fixed at the bulk-relaxed values, to prevent the surfaces collapsing across the void. The atoms in the slab itself are of course allowed to relax during the calculation.

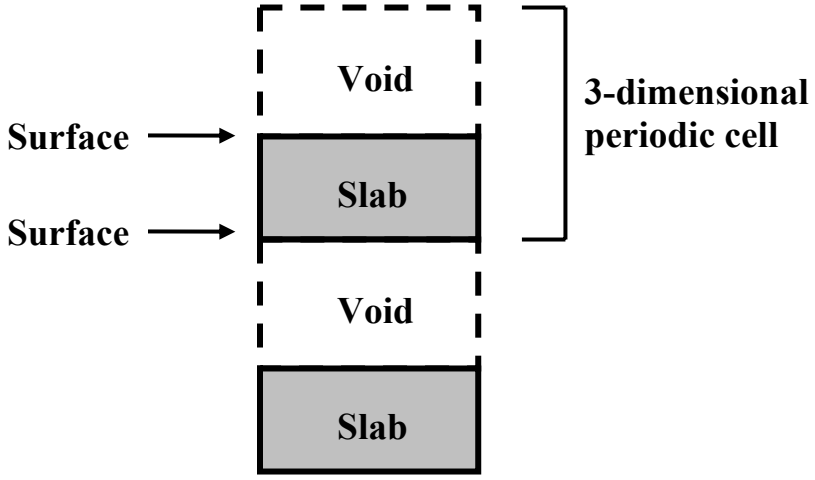


***Figure 4***. *Schematic representation of the three-dimensional surface simulation cell.*

## 3. Surface Defects

Just as there are two approaches to the modelling of surfaces, either employing a two- or three-dimensional periodic simulation cell, similarly there are also two approaches to the modelling of surface defects, such as vacancies or adsorbates at the surface.

### *3.1. Supercell approach*

In most computer simulation codes, such as METADISE (Watson et al., 1996) and VASP (Kresse and Hafner, 1993, 1994a; Kresse and Furthmueller, 1996a, 1996b) used in this work, any defects in the bulk or on the surface are periodically repeated throughout the crystal. As this periodic repeat may give rise to unnaturally large concentrations in the crystal, large supercells made up of multiple simulation cells are

used to model defects at low concentration. However, especially with computationally intensive calculations, the size of the supercells is limited by the available computational resources and often smaller than is required to give a realistic defect concentration. Some codes therefore employ an alternative approach, whereby the defect is truly isolated and embedded within a perfect crystal, hence simulating defects at infinite dilution.

### *3.2. Isolated defects*

One code which allows for the modelling of isolated surface defects, such as charged vacancies or adsorbed molecules, is CHAOS, a surface simulation code developed by Duffy and Tasker (1984) which calculates the structures and energies of point defects at the surface of crystals. In this code the crystal is again divided into a region I and a region II. Region II is further subdivided into two regions, IIa and IIb. In this case the regions are hemispheres centred upon the point defect on the surface (Figure 5).

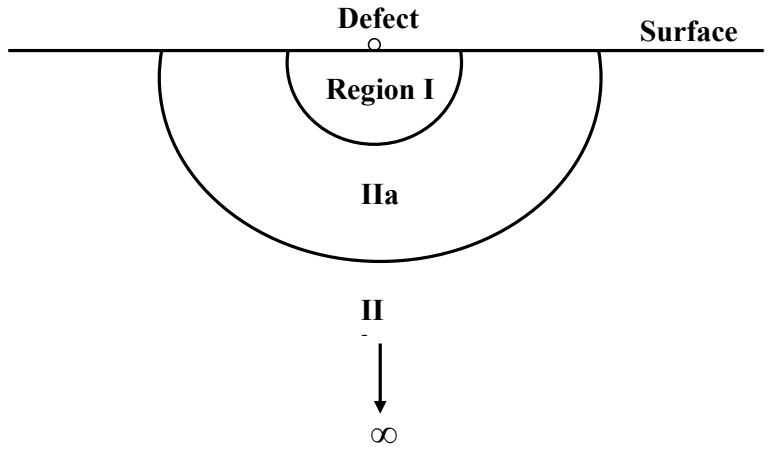


***Figure 5***. *Isolated Defect*

The interactions between ions in region I and region IIa are calculated explicitly just like the interactions between the ions in regions I and II described above. The interactions between region I and the rest of the crystal are approximated (Mott and Littleton, 1938, 1989) assuming the rest of the crystal is a dielectric continuum. In addition, the defect at the surface, which is a dielectric discontinuity, creates a dipole which induces dipoles in region IIb. The interactions between region I and IIb are therefore modified to include these charge induced dipoles. These approximations assume that the effect of the defect on the local geometry of the crystal is only

noticeable in the immediate surroundings of the defect but that the energy of the rest of the crystal is modified by the charged defect. The total energy of the system therefore consists of three terms:

$$U(\underline{x},\underline{y}) = U_1(\underline{x}) + U_2(\underline{x},\underline{y}) + U_3(\underline{y}) \quad (4)$$

where $U_1(\underline{x})$ is the energy of region I, $U_3(\underline{y})$ is the energy of region II and $U_2(\underline{x},\underline{y})$ is the energy of interaction between regions I and II. The vectors $\underline{x}$ and $\underline{y}$ represent the coordinates of the ions in region I, which are calculated explicitly, and the displacements in region II, respectively. As $U_3(\underline{y})$ contains an infinite number of displacements, it cannot be solved exactly and we need to make assumptions. We assume that the distance between the defect and the innermost region of region II is large enough to consider the outer region to equal the perfect crystal. The charge induced dipoles due to the defect cause harmonic displacements of the ions only and hence $U_3(\underline{y})$ can be represented by a quadratic function of $\underline{y}$:

$$U_3(\underline{y}) = \frac{1}{2}\underline{y}\underline{\underline{A}}\underline{y} \quad (5)$$

where $\underline{\underline{A}}$ is the force constant of the harmonic displacement. At equilibrium, when $\underline{y} = \underline{\bar{y}}$, the total force which is the derivative of the total energy is zero and hence, when we substitute equation (5) into expression (4), we obtain:

$$\frac{\partial U(\underline{x},\underline{y})}{\partial \underline{y}} = \frac{\partial U_2(\underline{x},\underline{y})}{\partial \underline{y}} + \underline{\underline{A}}\underline{y} = 0 \quad (6)$$

If we multiply this equation by $\underline{y}/2$, this becomes:

$$-\left(\frac{\underline{y}}{2}\right)\frac{\partial U(\underline{x},\underline{y})}{\partial \underline{y}} = \frac{1}{2}\underline{y}\underline{\underline{A}}\underline{\bar{y}} \quad (7)$$

and thus, when $\underline{y} = \underline{\bar{y}}$ and the outer displacements are at equilibrium with a given set of displacements of the inner region we obtain an expression for the total energy as a function of $U_1(\underline{x})$ and $U_2(\underline{x},\underline{y})$ only:

$$U(\underline{x},\underline{y}) = U_1(\underline{x}) + U_2(\underline{x},\underline{y}) - \frac{1}{2}\frac{\underline{y}\partial U_2(\underline{x},\underline{y})}{\partial \underline{y}} \quad (8)$$

By iteratively minimising with respect to $\underline{x}$ until the forces on each ion in region I is

zero, *i.e.*:

$$\frac{\partial U(\underline{x},\underline{\underline{y}})}{\partial \underline{y}} = 0 \tag{9}$$

we obtain the total energy of the relaxed system including the defect. The energy is calculated in the same way as in equations (1-3) and the defect energy is then obtained from the difference between the energy of the perfect surface and that with point defect, obtained by CHAOS. One consequence of using CHAOS to calculate defects at surfaces rather than in the bulk is that the calculation of the ionic displacements and the energy of the continuum needs to be modified with respect to a bulk calculation. In a bulk calculation, the energy of the continuum is calculated by a $r^{-4}$ summation (where r is the distance from the defect), which assumes that away from the defect in region II there is no structural deviation from the perfect crystal structure. This is an unrealistic assumption when surfaces are concerned and the energy is therefore calculated as a sum of planar integrals around the surface for the planes in region I and II defined in figure 1 and a volume integral over the rest of the crystal. These planar integrals take explicit account of the dilation of the crystal at the surface and hence structural relaxation is allowed.

$$E_{IIb} = -\frac{Q^2}{2}(E_{planar} + E_{volume}) \tag{10}$$

$$E_{planar} = \sum_{p\in I,IIa}\sum_{j} q_j M_j \int_{(R_{IIb}^2 - r_p^2)^{1/2}}^{\infty} \frac{1}{(r^2 - r_p^2)} 2\pi r dr \tag{11}$$

$$E_{volume} = \sum_{j} q_j M_j \int_{R_{IIb}}^{\infty} \frac{1}{r^4} 2\pi r^2 dr \tag{12}$$

where Q is the total charge of region I, $q_j$ is the defect charge, $M_j$ is the Mott-Littleton displacement factor, $R_{IIb}$ is the cut-off radius, $r_p$ is the perpendicular distance from the origin to plane p and r is the distance from the defect. As noted above, an additional consequence of charged defects at surfaces is that a surface causes a discontinuity in the dielectric constant. As a result the charged point defect induces an image charge situated at half an inter-planar distance above the plane containing the defect. The field due to the image charge needs to be taken into account when calculating the ion displacements in region IIa and the polarisation energy of region IIb. This image charge interaction is given by:

$$q_i = q_{defect}\left(\frac{\varepsilon_1 - \varepsilon_2}{\varepsilon_1 + \varepsilon_2}\right) \tag{13}$$

where $q_{defect}$ is the net charge of the defect, $q_i$ is the charge of the image, $\varepsilon_1$ and $\varepsilon_2$ are the different dielectric constants of the adjoining materials and $\varepsilon_1 > \varepsilon_2$. When only surfaces in vacuum are considered, the value of $\varepsilon_2$ is usually set to 1, the value of free space.

## 4. Types of Surfaces

As noted in section 2. above, the crystal surfaces can be considered as a stack of planes. Tasker (1979) then identified three different types of surfaces: In a type I surface each plane has overall zero charge as it consists of both anions and cations in stoichiometric ratio (Figure 6a). A type II surface has a stacking sequence of charged planes but the repeat unit consists of several planes in a symmetrical configuration and as a result there is no dipole moment perpendicular to the surface (Figure 6b). As type I and type II surfaces have no dipole moment perpendicular to the surface the electrostatic energy converges.

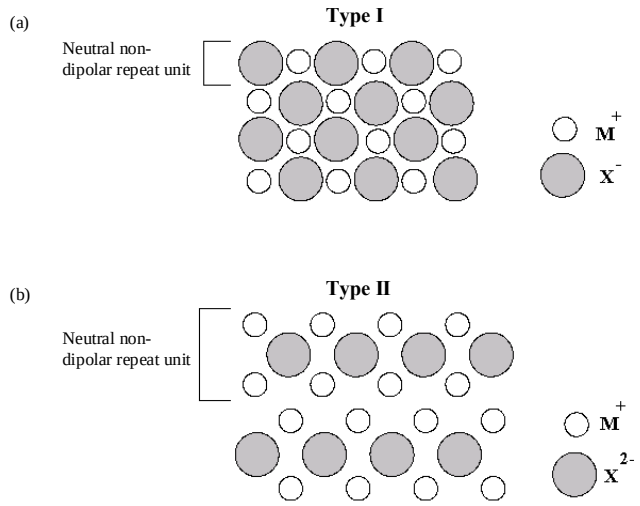


***Figure 6****. Stacking sequences showing type I surfaces consisting of charge neutral layers of positive and negative ions, and type II surfaces consisting of positively and negatively charged planes but with a charge neutral and non-dipolar repeat unit.*

Type III surfaces, however, are made up of a stack of alternately charged planes (Figure 7a), producing a dipole moment perpendicular to the surface. Bertaut (1958) showed that, when a dipole moment perpendicular to the surface is present in the unit

cell, the surface energy diverges and is infinite. In order to study this type of surface we need to remove the dipole. One way of achieving this is to remove half the ions from the surface layer at the top of the repeat unit and transfer them to the bottom (e.g. Oliver et al., 1993) (Figure 7b). As a result we obtain a surface which is partially vacant, either in cations or anions. These half-vacant planes are usually very unstable and are often particularly reactive towards impurity uptake or hydration (e.g. de Leeuw et al., 1995) or are found to reconstruct (e.g. Bowker et al., 2006). Once a surface is generated, which has no dipole moment perpendicular to the surface, the surface energy can be calculated.

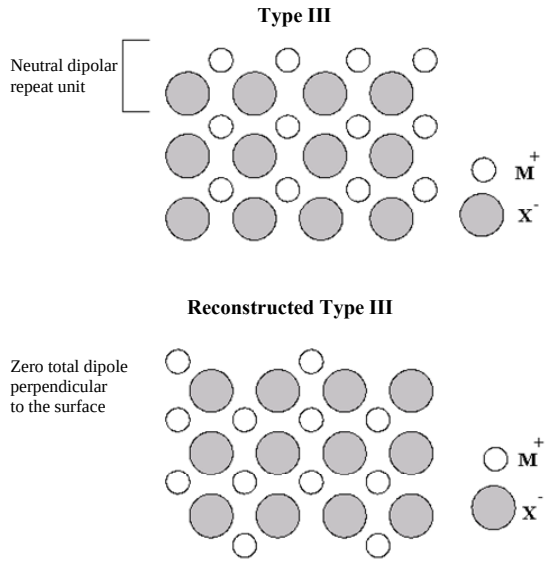


***Figure 7****. Stacking sequences showing a type III surface, consisting of alternating layers of positive and negative ions giving rise to a dipolar repeat unit, and a reconstructed Type III surface where half the surface ions have been shifted to the bottom of the unit cell, hence removing the dipole in the repeat unit.*

## 5. Surface Stabilities

The free surface energy of a plane is a measure of the stability of that particular surface, where a small, positive value indicates a stable surface. In this work, static lattice energy minimisations have been used, employing both electronic structure calculations and classical atomistic simulation techniques, to obtain bulk, surface and adsorption energies. The vibrational properties of the crystal are not taken into account and in effect the simulation is of a crystal at zero Kelvin ignoring the zero point energy. Although this may seem like an unrealistic approximation, nevertheless these simulations give good agreement with experiment (e.g. Tasker, 1979; Parker, 1983).

Furthermore, the vibrational and the zero point energy contributions to the surface free energies are small.

The excess energy for the surface has been defined by Stoneham (1976) as:

$$E_S = [\textit{cohesive energy of finite crystal}] - [\textit{number of atoms}] \text{ x } [\textit{cohesion energy per atom in infinite crystal}] \quad (14)$$

Throughout this work the surface energy $\gamma$ is then defined per unit area as follows:

$$\gamma = \left( \frac{E_S}{\text{Area}} \right) \quad (15)$$

In liquids this expression is equivalent to the surface tension since a liquid surface cannot support a stress (Harding, 1997). When stretching a liquid surface the number of atoms will increase to minimise the stress (Tasker, 1979).

The energies for surface and bulk blocks of the two-dimensional periodic crystal are evaluated using the approach outlined in section 2. The energy of block I comprising region I and II is the energy of the finite crystal containing the surface, and the energy of blocks I and II together yield the bulk energy or energy per atom in an infinite crystal. Regions I and II of both blocks need to be sufficiently large to ensure convergence of the surface energies. In the three-dimensional periodic slab/void system, the surface energy is simply the difference between the bulk and surface unit cell divided by the total surface energy, and convergence of the surface energy with slab thickness needs to be evaluated for each surface.

### *5.1. Crystal Morphology*

Gibbs (1928) proposed that the equilibrium morphology of a crystal should possess a minimum (free) energy for a given volume. According to Wulff's Theorem (1901), which is a variation of Gibbs theorem, the equilibrium shape of a crystal is determined by the surface energies of its various surfaces, in such a way that the equilibrium morphology is the shape of the crystal with minimum total surface free energy. Or, if the crystal is limited in space by n flat faces, then:

$$\frac{\sigma_1}{h_1} = \frac{\sigma_2}{h_2} = \ldots\ldots\ldots\ldots = \frac{\sigma_i}{h_i} = \frac{\sigma_n}{h_n} \quad (16)$$

where $\sigma_i$ is the specific free energy of the ith face and $h_i$ is the distance from the centre of the crystal to the plane of the ith face and is normal to the face (Tauson et al., 1993). Thus the height of a face is directly proportional to its specific free energy. Thus if two faces, for instance with directions [100] and [110], have the same specific free energy

they will have the same height. Figure 8 gives a schematic representation of the two surfaces where the bold line indicates the resulting equilibrium morphology.

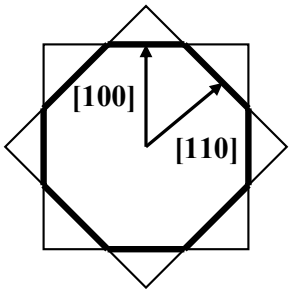


***Figure 8**. Schematic representation of two-dimensional equilibrium morphology due to two faces, (100) and (110), with equal specific free energy.*

At zero Kelvin, the specific free energy is a close approximation of the surface energy as calculated by static lattice simulations. Masri and Tasker (1985) found that the entropy term included in the surface free energy is small compared to the enthalpy term because the difference between the energies of the bulk and the surface is small. Thus the surface energies can be assumed to determine the equilibrium morphology of the crystal as follows:

$$E_S = \sum_i \gamma_i A_i = \textit{minimum for constant volume} \qquad (17)$$

where $E_S$ is as defined in equation (14) (Stoneham, 1976) and $\gamma_i$ and $A_i$ are the surface energy and surface area of the ith crystallographic face. Again, if two surfaces have the same surface energy and the same area, the morphology will be as in Fig. 8 above. However, in the more likely case that the surface energies and areas are different, the surface with the highest surface energy will grow out fastest resulting in a small surface area (or a long distance from the crystal centre), while the face with the lower surface energy grows more slowly, resulting in a large surface area (or short distance from the crystal centre), and hence will be expressed in the equilibrium morphology. Figure 9 illustrates this process.

This method of predicting crystal morphologies on the basis of thermodynamic factors has been very successful when the results were compared with experimentally found crystal shapes (de Leeuw and Parker, 1997). However, rather than being determined thermodynamically, experimental morphologies often depend on kinetic factors (Harding, 1997). Hartman and Bennema (1980) have tried to overcome this problem by assuming attachment energies are proportional to the growth rate for each surface and hence determine the kinetic morphology. In this simple phenomenological model, a slice of material is added to an already existing face on the bulk and the energy

released is the attachment energy, which is considered to be directly proportional to the growth rate (Woensdregt, 1992). Unfortunately, attachment energies assume bulk termination of the surface and do not take into account surface relaxation and reconstruction which was shown to be of utmost importance (e.g. Mackrodt et al., 1987). Gay and Rohl (1995) have attempted to address this problem by including the relaxation energy but it is unclear what this corresponds to within the attachment energy model. As such, although attachment energies are a useful and often successful concept, they are not as yet entirely satisfactory (Harding, 1976).

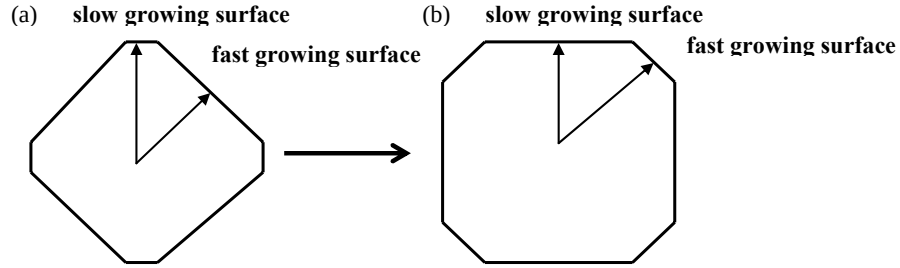


***Figure 9****. Schematic representation of the equilibrium morphology resulting from faces with different surface energies where (a) the initially large, fast growing surface in (b) has become small compared to the slow growing surface.*

## 6. A Case Study of α-Quartz $SiO_2$

In the remainder of this chapter we will discuss a case study of α-quartz $SiO_2$, where we have modelled the structure and stability of two different (0001) surface terminations and their interaction with water, including the onset of dissolution and the structuring effect of the surface on the liquid water at the interface. Accurate electronic structure calculations were used to investigate and compare the geometry and reactivity of the $SiO_2$ (0001) surface, whereas the same surface was modelled in liquid water by classical Molecular Dynamics (MD) simulations.

α-Quartz is one of the most abundant minerals at the Earth's surface, but in addition to its natural occurrence it is also important in electronic, optical and biomedical applications and unusual silica nano-structures have been synthesized by a variety of methods, from vapour deposition of silica thin films (Nishiyama et al., 2003), ribbons (Zach et al., 2003) and wires (Zhang et al., 2003) through the hydrothermal synthesis of quartz nano-crystals (Bertone et al., 2003) to templated sol-gel techniques for the production of smart silica nano-tubes for biomedical applications (Mitchell et al., 2002). As water is omnipresent in the environment, and crucially so at the stages of crystal

nucleation and growth, we have carried out an in-depth computational study of the quartz/water interface, using complementary simulation techniques.

### *6.1. Electronic Structure Calculations of the (0001) Surface*

The total energy and structure of two different α-quartz (0001) surface terminations were determined using the Vienna Ab Initio Simulation Program (VASP) (Kresse and Hafner, 1993, 1994a; Kresse and Furthmueller, 1996a, 1996b). The basic concepts of density functional theory (DFT) and the principles of applying DFT to pseudopotential plane-wave calculations are reviewed extensively in the literature and this methodology is now well established for the study of adsorbed atoms and molecules on the surfaces of ionic materials. Within the pseudopotential approach only the valence electrons are treated explicitly and the pseudopotential represents the effective interaction of the valence electrons with the atomic cores. The valence orbitals are represented by a plane-wave basis set, in which the energy of the plane-waves is less than a given cutoff ($E_{cut}$). The magnitude of $E_{cut}$ required to converge the total energy of the system has important implications for the size of the calculation when studying elements such as oxygen, which has tightly bound 2p electrons. The VASP program employs ultra-soft 'Vanderbilt'-like pseudo-potentials (Vanderbilt, 1990; Kresse and Hafner, 1994b), which allows a smaller basis set for a given accuracy. In our calculations the core consisted of orbitals up to and including the 1s orbital for oxygen and the 2p orbital for Si, whereas H has no core. The calculations were performed within the generalized-gradient approximation (GGA), using the exchange-correlation potential developed by Perdew et al. (1992).

α-Quartz has a hexagonal structure with spacegroup $P3_121$ and a unit cell of $a = b =$ 4.91Å, $c$ = 5.41 Å and $\alpha = \beta = 90°$ and $\gamma = 120°$ (Deer et al., 1992). In the DFT calculations, upon electronic and geometry optimisation, these lattice parameters contracted somewhat to $a = b$ = 4.85 Å, $c$ = 5.30 Å, but the calculated a/c parameter at 0.91 agrees within 0.9 % with the experimental value. The surface was modeled as a slab of material and separated by a vacuum gap from its images using three-dimensional periodic boundary conditions as described above. We have used two different terminations of the (0001) surface as starting configurations for our calculations, one plane where the bulk material was simply cleaved to give an (0001) surface with under-coordinated Si and O species (Figure 10a,b), and one (0001) plane where the under-coordinated surface species regained their bulk coordination by the formation of O-Si-O silanol bridges in the surface (Figure 10c,d). Both surfaces were then fully electronically and geometry optimized before calculating the surface energies of the two surfaces. When optimized, the bulk-terminated surface simply relaxed to a lower energy structure,

still with under-coordinated surface silicon atoms and oxygen dangling bonds. However, the case was less simple for the fully coordinated surface. This surface, where the oxygen dangling bonds are combined with the under-coordinated surface silicons to form four- and two-coordinated surface silicon and oxygen atoms respectively, was obtained spontaneously during geometry optimization of the bulk-terminated plane in interatomic potential-based simulations (de Leeuw et al., 1999). As such we were interested to calculate whether this termination of the {0001} surface is energetically more favourable than the surface with dangling bonds. We therefore relaxed a bulk-terminated slab in potential-based simulations and used the final surface structure as the starting configuration of our electronic structure calculations of the fully coordinated surface slab, which was then fully electronically and geometry optimized. We hence had obtained two fully optimised slabs with different surface terminations, as shown in Fig. 10, for comparison of the relative stabilities and reactivities towards water (Du and de Leeuw, 2004).

The electron density contour plots (through the planes containing species indicated by arrows in Figure 10) show that in all cases there is a significant distribution of the electron density along the Si-O bonds, both at the surfaces and in the bulk, indicating that the Si-O bond is not fully ionic but has a degree of covalency. From the side views in Figures 10(a) and (c) we see that in the fully coordinated surface (Figure 10c), the silicon and oxygen atoms of the second layer have moved up into the first layer to form the horizontal silanol bridges. Figure 10(d) shows a top view of this layer only with the electron density plot through the plane of the silicon atoms. The figure shows that the surface Si and O species form almost planar six-rings in the top layer, and that electron density of up to 0.26 $eÅ^{-3}$ is distributed along the Si-O bonds in a continuous network parallel to the surface. In the under-coordinated surface, however, despite contraction of the surface region as a whole, the second layer oxygen and silicon atoms have remained at different heights in the surface (Figure 10a), without the formation of a closed ring structure and no continuous network of electron density is found in the surface layer (Figure 10b). The surface energies for these surfaces were calculated to be 0.91 $Jm^{-2}$ for the fully coordinated plane and 2.28 $Jm^{-2}$ for the under-coordinated (0001) surface with dangling bonds, respectively. Clearly the fully coordinated (0001) quartz surface has a much lower surface energy than the under-coordinated surface, which is thus a local minimum energy structure rather than the lowest energy configuration of the anhydrous quartz surface, and the fully coordinated surface with the silanol bridges is the more stable structure.

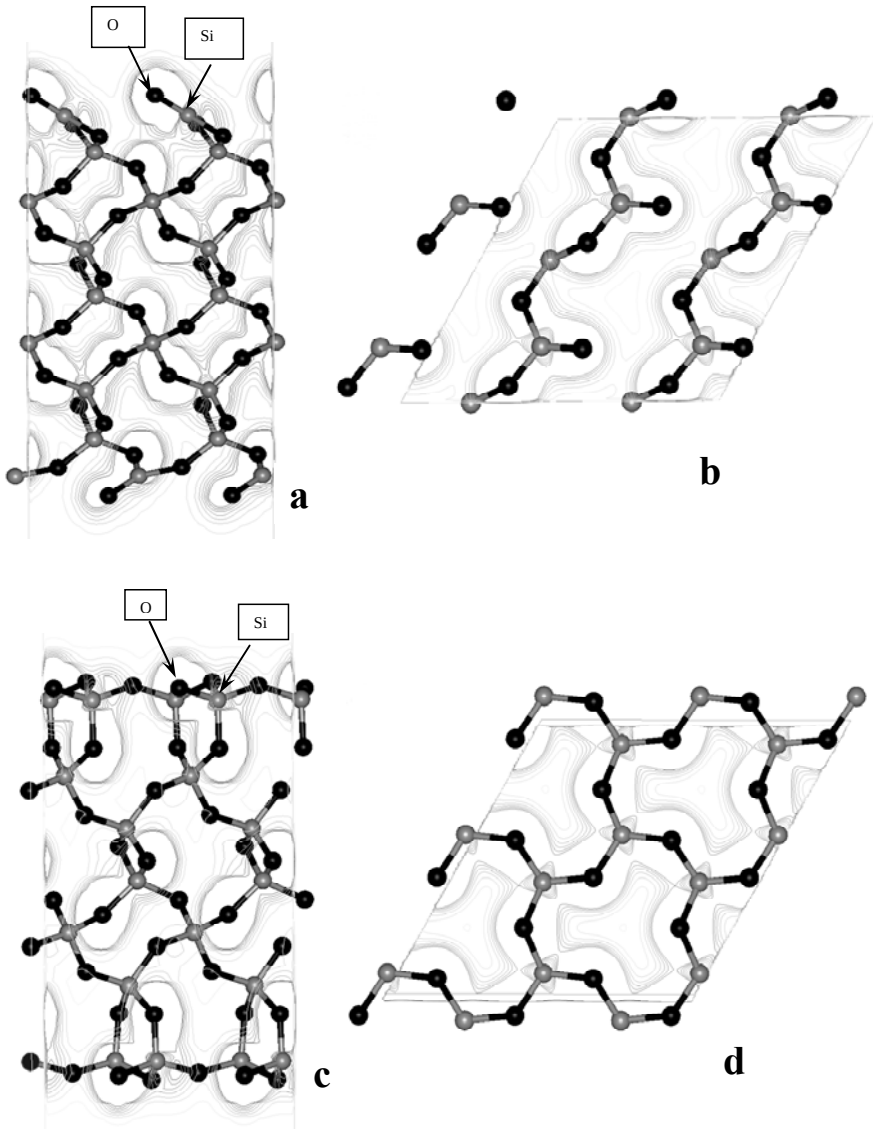


***Figure 10**. Side (a) and top (b) view of the geometry optimized under-coordinated (0001) surface, and side (c) and top (d) view of the geometry optimized fully-coordinated (0001) surface, showing electron density contour plots through planes containing surface Si and O as indicated on the side views, (a) and (c), and through the top silicon layer, (b) and (d) (Si = gray, O = black, contour levels from 0.02 to 0.26 eÅ$^{-3}$ at 0.04 eÅ$^{-3}$ intervals).*

We next introduced water molecules onto the two quartz surfaces. We first calculated adsorption of molecular water at the fully coordinated α-quartz surface, where we investigated a large number of initial configurations of the water molecule. In the

starting configuration leading to the lowest energy structure, the oxygen atom of the water molecule is attached to the surface silicon atom with a $Si\text{-}O_{water}$ distance of about 2.0 Å and distances between the hydrogen atoms of the water molecule and surface oxygen atoms of about 2.23 Å. The water molecule is initially located perpendicular to the surface with both hydrogen atoms of the water pointing away from the quartz surface, but after electronic and geometry optimization, the resulting structure (Figure 11) shows that at the fully coordinated α-quartz surface the water molecule rotates to lie almost flat upon the surface but does not dissociate upon adsorption. The water molecule remains associatively adsorbed with $Si\text{-}O_w$ and $O\text{-}H_w$ distances of 3.11 Å and 2.33 Å respectively. The electron density contour plots through a plane containing a surface silicon atom (and oxygen) as well as the water molecule's oxygen atom (Figure 11a) shows that the electron density is mainly centered on the ions and there is no significant electron density distribution along the $Si\text{-}O_w$ axis, indicating that the $Si\text{-}O_w$ interaction is distinctly different from the Si-O bonds in the crystal. In Figure 11(b) an electron density contour plot through a plane containing a surface oxygen and one hydrogen of the water molecule is shown, where some charge density is distributed along the O---H axis (up to 0.07 $eÅ^{-3}$) indicating weak hydrogen-bonding by the water molecule to the surface oxygen. No formal chemical bonds have formed between the surface and water molecules and the adsorption appears to be associative physisorption with hydrogen-bonding between hydrogen and surface oxygen.

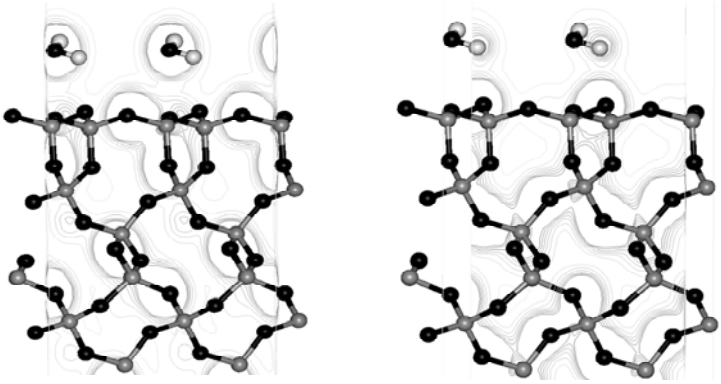

***Figure 11***. *Geometry optimized structure of the fully coordinated (0001) surface slab with associatively adsorbed water molecules, showing electron density contour plot through a plane containing (a) both a surface silicon atom and the oxygen atom of the water oxygen, and (b) a surface oxygen atom and one of the hydrogen atoms of the water molecule (Si = gray, O = black, H = white, electron density contour levels from 0.02 to 0.22 e $Å^{-3}$ at 0.04 e $Å^{-3}$ intervals).*

We investigated whether dissociation of the water molecule would be energetically preferred but hindered by an activation energy, by adsorbing dissociated water molecules at the surfaces, i.e. attaching a hydroxy group to a surface silicon atom and a hydrogen atom to a surface oxygen atom, before allowing the system to optimize. However, the initially dissociated surface OH groups recombined to form associated water molecules, hence clearly showing that associative adsorption is the preferred mode of adsorption of water at the fully coordinated (0001) surface. This molecular adsorption is an exothermic process releasing 45.3 kJ $mol^{-1}$, which relatively small hydration energy also indicates the weak physisorption of the water at the surface.

We next investigated the adsorption of water molecules at the under-coordinated (0001) surface. Upon full electronic and geometry optimization, the water molecule dissociated, with the formation of two OH groups on the surface (Figure 12), indicating that there is no significant energy barrier to the dissociation of a water molecule. It is clear from Figure 12, showing electron density contours through the plane of surface silicon atoms and the oxygen atoms of the hydroxy groups, that significant electron density is distributed along the Si-OH bond indicating covalent character just like the Si-O bonds in the silicate structure. Likewise, the O-H bond is also semi-covalent as is evident from the electron density contour plot through the O-H plane in the hydroxy groups, which is similar to OH groups in other materials (de Leeuw, 2001). In addition, Figure 12 shows that there is also electron density distributed between the hydrogen of one hydroxy group to the oxygen of the second group, indicating hydrogen-bonding between the hydroxy groups. This dissociative chemisorption, terminating the dangling bonds of the under-coordinated Si and O species by OH groups is far more exothermic than the molecular adsorption at the fully coordinated surface described above with an adsorption energy of –140.7 kJ $mol^{-1}$. The higher reactivity of the under-coordinated surface towards water is most likely due to termination of the dangling bonds, where the hydrated surface now contains only fully coordinated surface species. The same preference by under-coordinated species on silicate surfaces to be capped by hydroxy groups was shown in interatomic potential-based calculations of quartz and vitreous silica surfaces (de Leeuw et al., 1999; Rustad et al., 1998). If the water had adsorbed in a molecular fashion, the surface Si and O atoms would have remained under-coordinated, which as we saw for the anhydrous surfaces is a highly unstable configuration. Termination of the dangling bonds and hence increasing the coordination of the surface species is thus the driving force behind the dissociation of the adsorbed water molecules, aided by the formation of the residual hydrogen-bonding between the hydroxy-groups which further stabilises the hydrated surface.

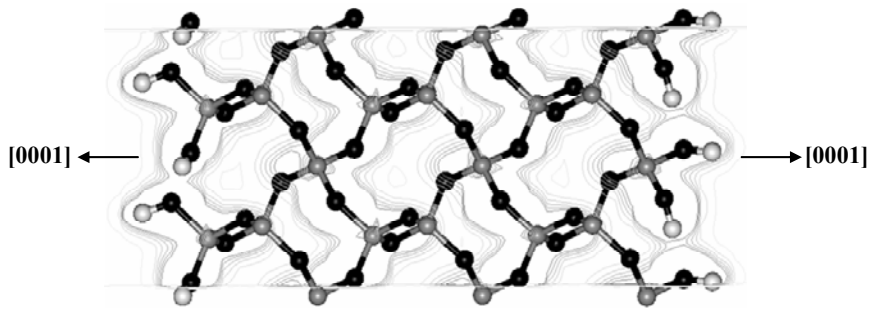


***Figure 12**. Geometry optimized structure of the under-coordinated (0001) surface slab with dissociatively adsorbed water molecules terminating the dangling bonds, showing electron density contour plot through a plane containing a surface silicon atom (Si = gray, O = black, H = white, electron density contour levels from 0.02 to 0.22 e $Å^{-3}$ at 0.04 e $Å^{-3}$ intervals).*

The calculated surface energies of the hydrated surfaces are now 1.08 $Jm^{-2}$ for the hydrated fully coordinated (0001) surface and 0.12 $Jm^{-2}$ for the hydrated (formerly) under-coordinated surface respectively. In the case of the fully coordinated surface, the stability of the surface has decreased upon hydration as shown by the increased surface energy. This decreased stability is probably due to the fact that the dry surface is already a stable plane with all surface species having their bulk-coordination numbers. Addition of the adsorbed water molecules only serves to make the surface less smooth, and disrupts the network of electron density along the planar six-rings in the surface, leading to the decrease in stability. Conversely, for the under-coordinated surface, the surface energy of the hydrated surface is much smaller than that of the dry surface and this plane has now become the preferred termination of the (0001) surface. The reason for this stability lies in the structure of the hydrated surface. The oxygen atoms of the hydroxy groups that become attached to the surface silicon atoms, fill positions on the surface that would be taken by oxygen atoms in the silica lattice if a new layer of material was grown on the surface, which can be seen in figure 12 if we compare the $SiO_4H_2$ groups at the surfaces with the equivalent $SiO_4$ groups in the bulk material. The hydrogen atoms complete the coordination of the surface oxygen atoms and to a certain extent mimic bulk Si atoms by bridging to a second oxygen through hydrogen-bonding.

### *6.2. Molecular Dynamics Simulations of the (0001) Surfaces in Liquid Water*

The accuracy of potential-based simulations is largely dependent on the quality of the interatomic parameters. In the simulations, we have used the $SiO_2$ potential model of Sanders et al. (1984), the Si-OH parameters optimized by Baram and Parker (1996) and

the water potential model by de Leeuw and Parker (1998), all of which employ the shell model of Dick and Overhauser (1958) to include polarisability of the oxygen ions. A similar combination of these potential models has previously been used successfully in a study of hydration of quartz surfaces (de Leeuw et al., 1999), but we decided to repeat the DFT calculations using the same simulation cell to gain information on the agreement or discrepancy between the methods. In all cases, the thickness and the gap width of the surfaces as well as the initial position of the water molecule is the same as that in the DFT calculations, unlike the simulations in de Leeuw et al. (1999). At the fully coordinated surface, associative adsorption of the water molecules was preferred similar to the DFT calculations. Using the potential model from de Leeuw et al. (1999), the energy of adsorption was calculated to be -105.1 kJmol$^{-1}$ and the Si-$O_{water}$ distance was found to be 1.79 Å, indicating that the surface silicon atom has now become coordinated to five oxygen atoms, which is clearly unrealistic. Compared to the DFT calculation of the same system, both the structure and hydration energy of the potential-based simulation indicates that the interaction between the water molecule and the surface is too strong. However, a minor refinement of the potential between the silicon atom and oxygen atom of the water, gave a much closer agreement between the two methods with a calculated energy of hydration of –56.9 kJ mol$^{-1}$, which at a difference of 11.6 kJ mol$^{-1}$ is in acceptable agreement with the DFT calculation. The distance between the water oxygen atom and the surface silicon and the distance between hydrogen atom and surface oxygen atom are 2.82 Å and 2.08 Å respectively compared to 3.11 Å and 2.33 Å for the equivalent DFT calculation. Although the water molecule in the potential-based simulation is still adsorbed more strongly to the surface, the agreement between the methods is certainly acceptable taking into account the necessary approximations employed in both methods (Du and de Leeuw, 2004).

The computer code used for the MD simulations was DL_POLY version 2.13 (Smith and Forester, 1996), where the integration algorithms are based on the Verlet leap-frog scheme (Verlet, 1967). In MD simulations, there are two ways to treat the shells that are essentially massless: either performing an energy minimization of shells only at each time step (Lindan and Gillan, 1993) or the approach used in DL_POLY, where a small mass is assigned to the shells (Mitchell and Fincham, 1993; Ferneyhough and Fincham, 1994). In this study, we have chosen a mass of 0.2 a.u. for the oxygen shell, which is small enough compared to the mass of the hydrogen atom of 1.0 a.u. to avoid energy exchange between the vibrations of oxygen core and shell and the oxygen and hydrogen vibrations. Due to the use of a shell model for oxygen, we need to use a small time step of 0.2 fs to maintain a stable system. The simulations were initially performed using NVE and NVT (constant number of particles, constant volume and constant energy or temperature) ensembles to equilibrate the system for 10000 timesteps, followed by both

equilibration and the final data collection runs at NPT (constant number of particles, constant pressure, constant temperature) for at least 100 ps at temperatures of 250, 300K and 350K. The Nosé-Hoover algorithm (Nosé, 1984; Hoover 1985) was used for both NVT and NPT ensembles with the thermostat and barostat relaxation times for the Nosé-Hoover parameters both set at 0.5 ps. The production run produces a range of properties of the system at each timestep, including structure, temperature, volume and energy, as well as the averaged properties and root mean square deviations. In order to investigate the hydration and dissolution of the $\alpha$-quartz (0001) surfaces in a liquid water environment, we built a simulation cell comprising a (4 x 4 x 4) slab of quartz crystal terminated by one hydroxylated surface (as in Figure 12) and one fully coordinated surface with O-Si-O bridges (Figure 11), separated from its images by a block of 360 water molecules which was kept at the simulated equilibrium water density of 1.3 g/cm (de Leeuw and Parker, 1998).

The analysis of the resulting structure shows that near the surface capped by the OH groups, the water behaves like liquid water where the molecules are distributed randomly in three dimensions (bottom of Figure 13a), whereas several ordered mono-layers of water are formed near the bridged surface, well separated from each other, where the water molecules are clearly orientated with respect to the surface (top of Figure 13a) (Du and de Leeuw, 2006). The reasons for the different water patterns at the two different surfaces are probably two-fold. Firstly, the surface structure of the quartz substrate obviously plays a rôle. The surface species in the bridged surface are more highly charged and the interfacial water molecules interact with the surface via attractive electrostatic interactions between surface silicon atoms and water oxygen atoms, as well as between surface oxygen atoms and hydrogen atoms of the interfacial water molecules. The ring structure on the bridged surface shown in Fig.10b contributes to the ordering of the nearest layer of the interfacial water molecules at the surface, as the locations of the surface Si and O species are well defined, forcing the adsorbed water into a regular pattern. The mono-layers of water molecules on the bridged surface are formed at an early stage and once the system reaches equilibrium the water molecules within each individual layer remain in their layer and no exchange of water molecules takes place between neighbouring layers. Once formed, the mono-layers of water molecules on the bridged surface are stable, especially at lower temperatures (250K, 300K). Analysis shows that at lower temperature (e.g. 250K) the mono-layer next to the substrate exhibits ice-like features, such as a complete network of hydrogen-bonded interactions between the water molecules in a regular pattern, which does not appear at higher temperature or in the mono-layers further away from the surface.

In order to quantify the layering of the water molecules above the surface, in Figure 13(b) we have plotted a diagram showing the distance between the surface, which we have defined here as the topmost surface silicon atom and the oxygen atom of each water molecule. Figure 13(b) clearly shows the distinct layering of the water molecules in the first three layers with a narrow band for the Si-O distances in each layer. This layered structure becomes less pronounced in the fourth layer, where there is no longer a clear gap between it and the next layer of water, and it is lost completely at distances further away from the surface than about 15 Å.

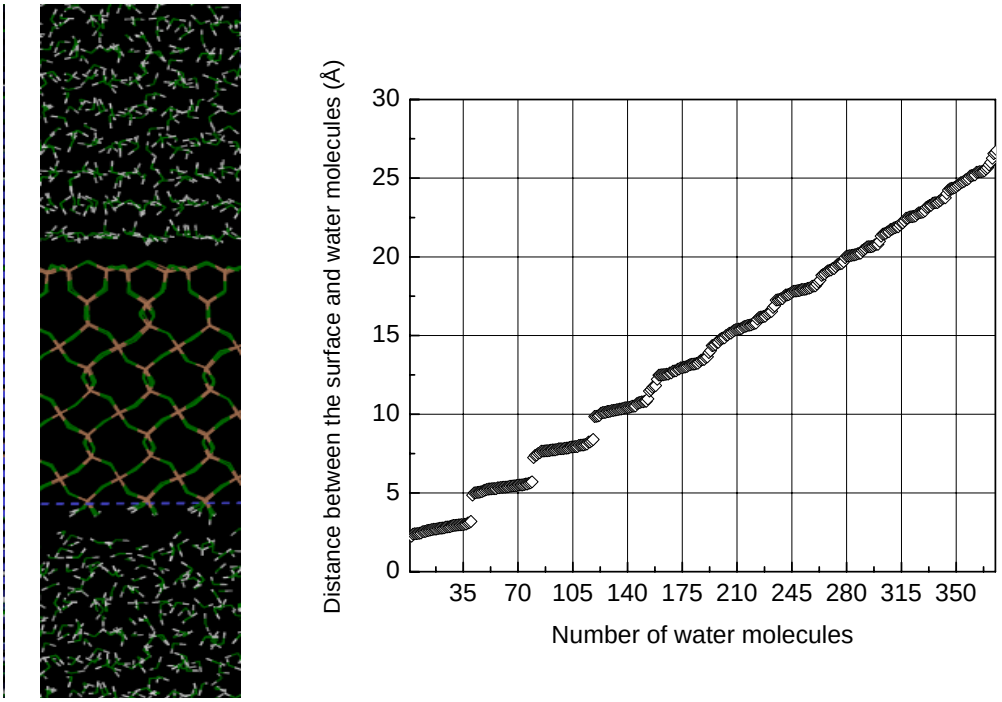


***Figure 13**. (a) Snapshot of the structure of the interfacial water molecules near the OH-capped and Si-O-Si bridged surface at 300K, and (b) diagram showing the Si-$O_{water}$ distance for all water molecules with respect to the surface.*

Unlike the bridged surface, there is no ring structure or strong electrostatic field at the surface terminated by OH groups. The surface species, i.e. the hydroxy groups of the silanol groups, are relatively flexible compared to the surface species of the bridged surface and the interfacial water molecules loosely associate with the surface via hydrogen-bonding between the oxygen atoms of the interfacial water molecules and hydrogen atoms of the surface hydroxy groups. In terms of configuration and bonding,

the surface hydroxy groups more closely resemble water molecules themselves and a relatively disordered three-dimensional interfacial water region forms near the surface, similar to bulk liquid water (bottom of Figure 13a). We have calculated relevant O-O and O-H radial distribution functions (RDF) for the water molecules, which show that the water indeed acts like bulk liquid water, with an O-O first peak at 2.97 Å (height 3.75) and a second peak at 5.3-5.5 Å (height 1.24), in excellent agreement with simulations of bulk water using the same potential model (2.97 and 5-6 Å, heights 3.8 and 1.3) (de Leeuw and Parker, 1998) and experiment (2.88 and 4.6 Å, heights 3.1 and 1.1 (Narten and Levy, 1971; Soper and Phillips, 1986). The O-H RDF shows a first peak at 2.1 Å (height 0.90) and a second maximum at 3.2 Å (height 1.31), again identical to the earlier MD simulations of liquid water (de Leeuw and Parker, 1998) and in good agreement with experiment which shows maxima at 1.9 and 3.2 Å (heights 1.0 and 1.3, respectively) (Soper and Phillips, 1986). This liquid-like behaviour is in agreement with experimental findings of interfacial water near the quartz surface at low pH, i.e. when surface silanol groups are present (Ostroverkhov et al., 2004, 2005).

### *6.3. Dissolution of silicic acid $Si(OH)_4$ from the (0001) surface*

We next investigated the dissolution of a silicon species from the OH-capped quartz surface in a liquid water environment. A series of molecular dynamics calculations was carried out using NVE, NVT and NPT equilibration and NPT data collection runs at 300 K and 1 atm. The property we need to obtain from our MD simulations is the energy of dissociative hydration of various Si-O bonds at the surface, which is the energy released per water molecule upon adsorption of dissociative water at the relevant Si and O atoms in the quartz surface. This $E_{hydration}$ is calculated from the following energy cycle:

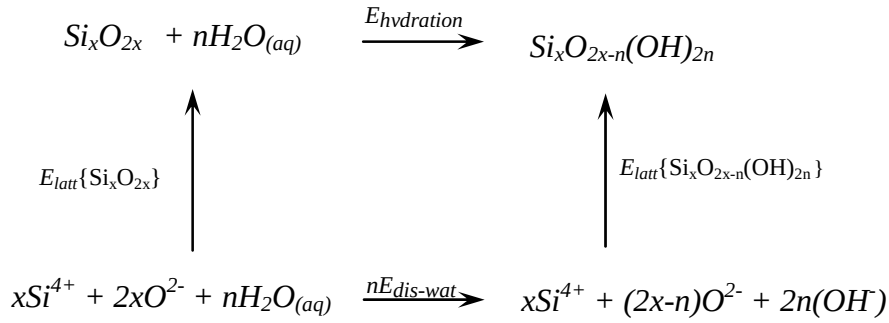


(18)

where $Si_xO_{2x}$ is the system before hydration of the surface Si-O bond and $Si_xO_{2x-n}(OH)_{2n}$ is the system after hydration of the Si-O bond. All the reactions here take place in a liquid water environment, where $E_{hydration}$ is the hydration energy of dissociative

adsorption of water at the surface, $E_{latt}\{Si_xO_{2x}\}$ is the calculated energy of the cell before the hydration took place, $E_{latt}\{Si_xO_{2x-n}(OH)_{2n}\}$ is the energy of the cell after the dissociative adsorption of $n$ water molecules at the surface Si-O bond. In order to calculate $E_{hydration}$ we need one other energy that cannot be obtained directly from the MD simulations, namely $E_{dis\text{-}wat}$, which is the energy of dissociation of the water molecule at the surface, which is material dependent. However, this property can also be obtained from an energy cycle, using experimental enthalpies for some of the reactions, as shown in equation (19):

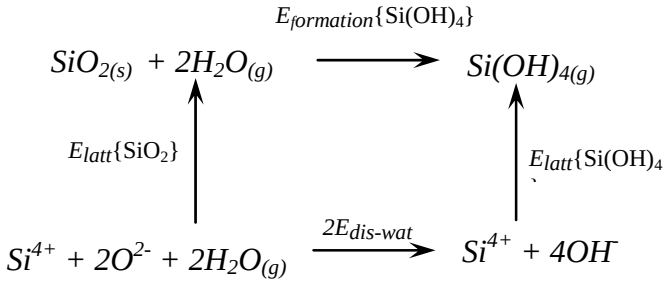


(19)

As $E_{dis\text{-}wat}$ involves an $O^{2-}$ species, there is no absolute energy for this reaction as the second electron affinity of oxygen is material dependent and we hence need to calculate the value for an Si-O-H system, in this case silicic acid $Si(OH)_4$, which is a pre-cursor gel to many silicate materials and is found extensively in seawater (Greenwood et al., 2005). $E_{formation}\{Si(OH)_4\}$ is the experimental heat of formation of silicic acid $Si(OH)_4$ which was found to be 11.5 kJmol$^{-1}$ (Ramberg, 1954; Greenberg, 1957), $E_{latt}\{Si(OH)_4\}$ and $E_{latt}\{SiO_2\}$ are the lattice energies of $Si(OH)_4$ and $SiO_2$, which were calculated to be –10734.0 kJ mol$^{-1}$ and –12402.2 kJ mol$^{-1}$ at 300K, respectively. According to energy cycle (19) and the enthalpy of vaporization of water at 300K, the reaction of one lattice oxygen with one water molecule to form two hydroxy group thus releases 828.3 kJ mol$^{-1}$, which is the $E_{dis\text{-}wat}$ energy we need to include in our calculation of the energy of dissociative adsorption of water at the surfaces, $E_{hydration}$, which is the quantity that we are interested in. This same procedure has been used in previous studies of the dissociative hydration of oxide surfaces, and has been shown to give good agreement with experiment (de Leeuw et al., 1999; de Leeuw et al., 2003; Du and de Leeuw, 2004, 2006).

We first calculated the energy of adsorption of dissociated water molecules at the dangling bonds of the Si and O atoms in the anhydrous surface. This hydration energy is calculated, according to equation (18), at $\Delta H$ = –157 kJ mol$^{-1}$. For comparison we have also run similar simulations of hydration of the surface with dangling bonds *in vacuo*,

where the surfaces are separated by a void, and the calculated hydration energy is then $\Delta H = -177$ kJ mol$^{-1}$ (in fair agreement with the DFT calculations above taking into account the wholly different simulation conditions). The difference in the hydration enthalpies between liquid water and vacuum indicates that dissociative adsorption of a water molecule under vacuum conditions is energetically more favorable than in a liquid water environment. Under vacuum conditions, the OH groups bonded to the surface of the substrate only interact with surface silicon and oxygen atoms. However, when the dissociative adsorption takes place in a liquid water environment, the OH groups not only interact with surface atoms of the substrate but also with interfacial water molecules, which causes the OH groups to be less strongly attracted to the surface. In addition, the vacuum interface is less stable (surface energy $\gamma = 1.65$ Jm$^{-2}$) and hence more reactive than the liquid water interface ($\gamma = 1.46$ Jm$^{-2}$) (Mijoule and Bouteiller, 1991). Dissociative adsorption in a liquid water environment is therefore slightly less energetically favourable.

On the hydroxylated (0001) surface, each surface Si atom is already bonded to two OH groups from the earlier hydration of the surface with the formation of two geminal hydroxy groups. To simulate the further dissolution of the Si species from the quartz surface in a liquid water environment, we have sequentially added two more dissociated water molecules to one of the hydroxylated surface silicon atoms, as shown in equation (20), where addition of each water molecule adds another OH group to the silicon and a proton to a neighbouring oxygen atom associated with the silicon atom:

$$[Si(OH)_2]_{Si} + 2H_2O_{(aq)} = 2H_{Si} + Si(OH)_{4(g)} \qquad (20)$$

where $[Si(OH)_2]_{Si}$ is a $-Si(OH)_2$ species located at a Si site of the (0001) quartz surface, i.e. a surface Si atom on the hydroxylated surface which is bonded to two hydroxy groups, and $H_{Si}$ is a proton adsorbed at this silicon site.

Eventually, the silicon is bonded to four OH groups and hence a free $Si(OH)_4$ species is released from the surface, leaving four protons at the quartz surface to replace the dissolved Si atom., as shown in Figure 14. This process, where a Si atom is replaced by four protons, is a well-known defect structure in the bulk of many silicate materials, although not surprisingly it was calculated to be thermodynamically unstable in the bulk of pure $\alpha$-quartz at low temperatures (de Leeuw 2001, Rosa et al. 2005).

Hydrolysis of the first Si-O bond leads to the breaking of one of the remaining two Si-O bonds linking the surface silicon atom with two non-surface neighbouring oxygen atoms deeper into the bulk material (Fig. 14a). To this end, a third OH group is adsorbed to the surface silicon and a proton to one neighboring oxygen atom, which thus leads to

a non-surface silicon atom at a lower level becoming capped by an OH group (Fig. 14b). Meanwhile the $Si(OH)_3$ species formed at the surface remains approximately at the original site of the $Si(OH)_2$ and the whole structure of the quartz surface at this stage remains almost unchanged, except for the formation of this $Si(OH)_3$ at the surface. When a second dissociated water molecule is adsorbed to the silicon atom, the last Si-O bond is broken and a $Si(OH)_4$ species is formed. From Figure 14c, it is clear that the $Si(OH)_4$ species has moved away from the original position of the silicon atom into the liquid water and a surface $Si(OH)_2$ vacancy has been created, which is charge compensated by two protons. The basic structure of the quartz surface surrounding the defect is not significantly disrupted, apart from a degree of relaxation of a few surface atoms into the bulk. The reason for this lack of reconstruction of the surface upon the dissolution of the $Si(OH)_4$ species is the absence of strain in the original surface, which is in stark contrast to the dissolution process of a Si atom from the end of a silica nanotube [de Leeuw et al. 2003], where significant disruption was observed on release of $Si(OH)_4$ due to the strained nature of the Si-O bonds.

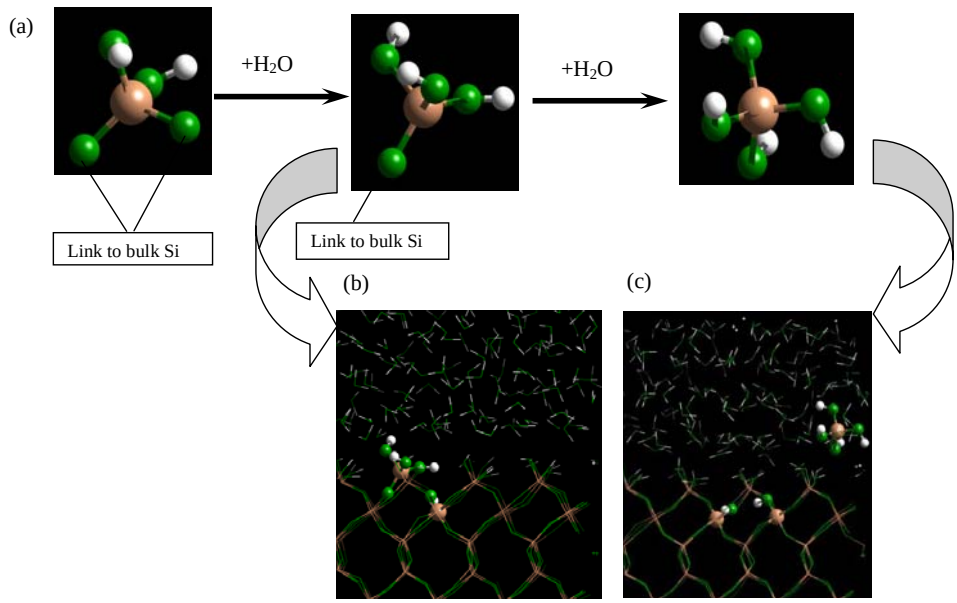


***Figure 14***. *Details of the stepwise dissolution of a Si(OH)4 molecule from the hydroxylated α-quartz (0001) surface*

*6.4. The Effect of Entropy in the Dissolution Process*

When we calculate the consecutive adsorption of the two dissociated water molecules to the surface silicon atom, addition of the first water molecule to the surface $>Si(OH)_2$ species, leading to a surface $-Si(OH)_3$ group, releases -56.0 $kJmol^{-1}$. However, addition of the second water molecule with the formation of a detached $Si(OH)_4$ species is less straightforward. When the $Si(OH)_4$ remains close to the quartz/water interface, as shown in figure 14c, the process is energetically unfavourable, costing 40.0 kJ $mol^{-1}$. This energy penalty increases further if the $Si(OH)_4$ molecule is moved away from the defective surface, for instance, into the bulk region of the water, when the last step in the dissolution process becomes energetically even more expensive at 58.8 kJ $mol^{-1}$. These calculated energies show that although the complete two-step dissolution of a silicon species from a regular surface site on the quartz (0001) surface into liquid water is energetically favourable ($\Delta H$ = -16.0 $kJmol^{-1}$), the final Si-O bond hydrolysis step costs a significant amount of energy and may thus not occur.

However, the above energies for the dissolution process do not take into account entropy, and we therefore need to estimate how inclusion of entropic contributions to the energies could affect the viability of this process in liquid water. As discussed, the overall dissolution of a surface $>Si(OH)_2$ species to a free $Si(OH)_4$ silicic acid molecule in solution releases an enthalpy of 16 $kJmol^{-1}$, but in this process two water molecules from solution have become attached to either the quartz surface or the dissolved silicon atom, which would lead to a decrease in entropy, whereas the detachment of the silicon atom itself from the surface would lead to an increase in entropy. If we assume that the quartz surface remains largely unaffected through the loss of one Si atom, especially as the loss of its two existing OH groups to the silicic acid are compensated by the addition of two new OH groups at the surface, then we need only take into account the change in entropy due to the release of the free $Si(OH)_4$ molecule from the surface and the loss of two free water molecules from solution.

The entropy of quartz at 300K is 41.7 $Jmol^{-1}K^{-1}$ and that of liquid water (Lide, 2000) is 70.4 $Jmol^{-1}K^{-1}$. However, despite an extensive literature search we have not been able to find the experimental entropy of silicic acid in aqueous solution at ambient temperature, although some high-temperature gas phase values are known, and we have therefore used a calculated value for this property. Mora Fonz and coworkers have calculated entropies for a variety of silicate clusters and water, both in the gas phase and in solution (Mora Fonz et al., 2005). Their calculated entropy of gaseous water at S = 194.7 $Jmol^{-1}K^{-1}$ is in excellent agreement with experiment (S = 188.8 $Jmol^{-1}K^{-1}$) and they obtain a value for liquid water by using a cluster of water molecules in a dielectric field that gives a calculated value for the entropy of liquid water of S = 86.3 $Jmol^{-1}K^{-1}$,

which agrees less well with experiment, but is still a reasonable value. In view of the reasonable agreement between the calculated and experimental entropies for water, we can be confident that Mora Fonz et al.'s calculated values for the silicic acid species will be in similar agreement and this comparison also gives us a measure of the uncertainties in the calculated entropies. They calculated the entropy of the gas phase $Si(OH)_4$ species at ambient temperature to be S = 336.4 $Jmol^{-1}K^{-1}$, but the calculation of the molecule in solution is less straightforward. The dielectric field on its own had been shown to give poor results for a single liquid water molecule (calculated value S = 116.8 $Jmol^{-1}K^{-1}$), hence their use of the water cluster for the calculation of the entropy of liquid water. For that reason they also used a similar procedure for $Si(OH)_4$ in solution, by calculating the entropy of the molecule in a cluster of water plus the dielectric field, which gave them an entropy for the solvated $Si(OH)_4.4H_2O$ cluster of S = 453.3 $Jmol^{-1}K^{-1}$. Although this entropy is for the complete cluster in solution rather than the solvated silicic acid molecule itself, by including these extra four water molecules in the equation, we can obtain a value for the entropy of reaction (20). In addition, inclusion of the four extra water molecules in equation (20) is probably also more realistic as the water molecules surrounding the $Si(OH)_4$ species will have lost some of their freedom through this coordination to the silicic acid molecule, and hence their entropy will also have decreased (Haggis et al., 1952).

$$SiO_{2(s)} + 6H_2O_{(l)} \longrightarrow Si(OH)_4.4H_2O_{(aq)} \quad (21)$$

The entropy for reaction (21) is then calculated at $\Delta S$ = -106.2 $Jmol^{-1}K^{-1}$, which means that as $\Delta H$ = -16.0 $kJmol^{-1}$, at 300K the free energy of the dissolution process of one $Si(OH)_4$ species from the $\alpha$-quartz (0001) surface into water becomes $\Delta G$ = +15.9 $kJmol^{-1}$. The endothermicity of this process agrees with the fact that quartz is one of the most stable natural minerals and is found to be chemically resistant to most attacking solutions and insoluble in neutral water or acid under ambient conditions (Greenwood et al., 2005; Wang et al., 2004).

## 7. Conclusions

In this chapter we have described a variety of simulation methods to model a host of different surface and interfacial features and properties. We have illustrated some of these methods via a case study of $\alpha$-quartz where we have used the application of complementary computational techniques to elucidate the hydration behaviour of its dominant (0001) surfaces. Electronic structure calculations have shown how the geometry of the surface and in particular the coordination of the surface species is

crucial in determining the mode of adsorption of water, whereas classical MD simulations have illuminated the structuring of liquid water above the mineral surface. Calculations of the onset of dissolution of the quartz (0001) surface have shown that the inclusion of entropy is essential for the understanding of the subtle energetics of this important process.

The applications discussed in this chapter show how modern computer modelling techniques can now be applied routinely to investigate complex materials and processes, which are often difficult to study experimentally.

**Acknowledgements**

NHdL thanks the EPSRC for an Advanced Research Fellowship and acknowledges the EPSRC, NERC, Wellcome Trust and Royal Society for financial support.

**References**

Baram, P.S. and Parker, S.C. (1996) Atomistic simulation of hydroxide ions in inorganic solids. *Philosophical Magazine B* 73, 49-48.

Barrett, N.T., Guillot, C., Villette, B., Treglia, G. and Legrand, B. (1991) Inversion of the core level shift between surface and subsurgace atoms of the iridium (100) (1x-1) and (100) (5x-1) surfaces. *Surface Science* 251, 717-721.

Bertaut F. (1958) Le terme electrostatique de l'energie de surface. *Compt. Rendu.* 246, 3447-3450.

Bertone, J.F., Cizeron, J., Wahi, R.K., Bosworth, J.K. and Colvin, V.L. (2003) Hydrothermal synthesis of quartz nanocrystals. *Nano Letters* 3, 655-659.

Bowker, M., Stone, P., Fourrie, E., Ishii, M. and de Leeuw, N.H. (2006) The surface structure of BaO on Pt(111): (2x2)-reconstructed BaO(111). *Surface Science* 600, 1973-1981.

Colbourn, E.A., Mackrodt, W.C. and Tasker, P.W. (1983) The segregation of calcium ions at the surface of magnesium-oxide – Theory and calculation. *Journal of Materials Science* 18, 1917-1924.

Cooper, T.G. and de Leeuw, N.H. (2003) A combined *ab initio* and atomistic simulation study of the surface and interfacial structures and energies of hydrated scheelite: introducing a $CaWO_4$ potential model. *Surface Science* 531, 159-176.

Cooper T.G. and de Leeuw, N.H. (2004) A computer modelling study of the competitive adsorption of water and organic surfactants at surfaces of the mineral scheelite. *Langmuir* 20, 3984-3994.

Cooper, T.G. and de Leeuw, N.H. (2006) A computer modelling study of the incorporation of $K^+$, $Ca^{2+}$ and $Mg^{2+}$ impurities in two $NaSO_4$ polymorphs: Introducing a $NaSO_4$ potential model. *Journal of Crystal Growth* 294, 137-149.

Davies, M.J., Parker, S.C. and Watson, G.W. (1994) Atomistic simulation of the surface structure of spinel. *Journal of Materials Chemistry*, 4, 813.

de Leeuw, N.H. (2001) Density Functional Theory calculations of hydrogen-containing defects in forsterite, periclase and $\alpha$-quartz. *J. Phys. Chem. B* 105, 9747-9754.

de Leeuw, N.H. (2001) Local ordering of hydroxyl groups in hydroxy-apatite. *Chemical Communications* 17, 1646-1647.

de Leeuw, N.H. and Parker, S.C. (1998) Surface structure and morphology of calcium carbonate polymorphs calcite, aragonite and vaterite: an atomistic approach. *Journal of Physical Chemistry B* 102, 2914.

de Leeuw, N.H. and Cooper, T.G. (2003) A computational study of the surface structure and reactivity of calcium fluoride. *Journal of Materials Chemistry* 13, 93-101.

de Leeuw, N.H. and Cooper, T.G. (2004) A computer modeling study of the inhibiting effect of organic adsorbates on calcite crystal growth. *Crystal Growth & Design* 4, 123-133.

de Leeuw, N.H. and Parker, S.C. (1997) Atomistic simulation of the effect of molecular adsorption of water on the surface structure and energies of calcite surfaces. *Journal of the Chemical Society Faraday Transactions* 93, 467.

de Leeuw, N.H. and Parker, S.C. (1998) Molecular Dynamics simulation of MgO surfaces in liquid water using a shell model potential for water. *Physical Review B* 58, 13901-13908.

de Leeuw, N.H. and Parker, S.C. (2000) Modelling segregation of magnesium and cadmium ions to calcite surfaces: introducing $MgCO_3$ and $CdCO_3$ potential models. *Journal of Chemical Physics* 112, 4326-4333.

de Leeuw, N.H., Du, Z., Li, J., Yip, S. and Zhu, T. (2003) Computer modeling study of the effect of hydration on the stability of a silica nanotube. *Nano Letters* 3, 1347-1352.

de Leeuw, N.H., Higgins, F.M. and S.C. Parker, S.C. (1999) Modelling the surface structure and stability of α-quartz. *Journal of Physical Chemistry B* 103, 1270-1277.

de Leeuw, N.H., Nelson, C.J., Catlow, C.R.A., Sautet, P. and Dong, W. (2004) Density Functional Theory calculations of the adsorption of chlorine at perfect and defective silver (111) surfaces. *Physical Review B* 69, 045419

de Leeuw, N.H., Parker, S.C. and Harding, J.H. (1999) Molecular Dynamics simulation of crystal dissolution from calcite steps. *Physical Review B*, 60, 13792-13799.

de Leeuw, N.H., Parker, S.C., Catlow, C.R.A. and Price, G.D. (2000a) Proton-containing defects at forsterite {010} tilt grain boundaries and stepped surfaces. *American Mineralogist* 85, 1143-1154.

de Leeuw, N.H., Parker, S.C., Catlow, C.R.A. and Price, G.D. (2000b) Modelling the effect of water on the surface structure and stability of forsterite. *Physics and Chemistry of Minerals* 27, 332-341.

de Leeuw, N.H., Watson, G.W. and Parker, S.C. (1995) Atomistic simulation of the effect of dissociative adsorption of water on the surface structure and stability of calcium and magnesium oxide. *Journal of Physical Chemistry* 99, 17219-17225.

Deer, W.A., Howie, R.A. and Zussman, J. (1992) *An Introduction to the Rock-forming Minerals*, Longman.

Dick, B.G., Overhauser, A.W. (1958) Theory of the dielectric constants of alkali halide crystals. *Physical Review* 112, 90-103.

Du, Z. and de Leeuw, N.H. (2004) A combined density functional theory and interatomic potential-based simulation study of the hydration of nano-particulate

silicate surfaces, *Surface Science* 554, 193-210.
Du, Z. and de Leeuw, N.H. (2006) Molecular Dynamics simulations of hydration, dissolution and nucleation processes at the α-quartz (0001) surface in liquid water. *Dalton Transactions* 22, 2623-2634.
Duffy, D.M. (1986) Grain boundaries in ionic crystals. *Journal of Physics C: Solid State Physics* 19, 4394-4412.
Ferneyhough, R., Fincham, D., Price, G.D. and Gillan, M.J. (1994) The melting of MgO studied by molecular dynamics simulation. *Modelling and Simulation in Materials Science and Engineering* 2 1101-1110.
Filgueiras, M.R.T., Mkhonto, D. and de Leeuw, N.H. (2006) Computer simulations of the adsorption of citric acid at hydroxyapatite surfaces. *Journal of Crystal Growth* 294, 60-68.
Gay, D.H. and Rohl, A.L. (1995) MARVIN – A new computer code for studying surfaces and interfaces and its application to calculating the crystal morphologies of corundum and zircon. *Journal of the Chemical Society Faraday Transactions* 91, 925-936.
Gibbs, J.W. (1928) *Collected Works*, Longman.
Goniakowski, J. and Gillan, M.J. (1996) The adsorption of $H_2O$ on $TiO_2$ and $SnO_2$ (110) studied by first-principles calculations. *Surface Science* 350, 145-158.
Goniakowski, J., Holender, J.M., Kantorovich, L.N. and Gillan, M.J. (1996) Influence of gradient corrections on the bulk and surface properties of $TiO_2$ and $SnO_2$. *Physical Review B*, 53, 957-960.
Gorling, A., Ackermann, L., Lauber, J., Knappe, P. and Rosch, N. (1993) On the coadsorption of Co and alkali atoms at transition metal surfaces – A LCGTO-LDF cluster study. *Surface Science*, 286, 26-45.
Grau Crespo, R., Catlow, C.R.A., de Leeuw, N.H., (2007) Computer modelling study of redox processes at the $FeSbO_4$ (100) surface. *Journal of Catalysis* 248, 77-88.
Greenberg, S.A. (1957) Thermodynamic functions for the solution of silica in water. *Journal of Physical Chemistry* 61, 196-197.
Greenwood, J.E. Truesdale, V.W. and Rendell, A.R. (2005) Toward an understanding of biogenic-silica in seawater – An initial rate approach applied between 40 and 90 degrees C. *Aquatic Geochemistry* 11, 1-20.
Haggis, G.H., Hasted, J.B. and Buchanan, T.J. (1952) The dielectric properties of water in solutions. *Journal of Chemical Physics* 20, 1452-1465.
Harding, J.H. (1997) *Computer Modelling in Inorganic Crystallography*, ed. C.R.A. Catlow, Academic Press.
Hartman, P. and Bennema, P. (1980) The attachment energy as a habit controlling factor. 1. Theoretical considerations. *Journal of Crystal Growth* 49, 145-156.
Hoover, W.G. (1985) Canonical dynamics – Equilibrium phase-space distributions. *Physical Review A* 31, 1695-1697.
Kantorovich, L.N., Holender, J.M. and Gillan, M.J. (1995) The energetics and electronic structure of defective and irregular surfaces on MgO. *Surface Science* 343, 221-239.
Klepeis, J.E. and Terminello, L.J. (1996) Imaging of a surface state from clean Cu(001). *Physical Review B* 53, 16035-16040.

Kresse, G. and Furthmüller, J. (1996a) Efficiency of ab-initio total energy calculations for metals and semi-conductors using a plane-wave basis set. *Computional Materials Science*, 6, 15-50.

Kresse, G. and Furthmüller, J. (1996b) Efficient iterative schemes for ab initio total-energy calculations using a plane-wave basis set. *Physical Review B* 54, 11169-11186.

Kresse, G. and Hafner, J. (1993) Abinitio molecular-dynamics for liquic-metals. *Physical Review B* 47, 558-561.

Kresse, G. and Hafner, J. (1994a) Ab-initio molecular dynamics simulation of the liquid-metal amorphous semiconductor transition in germanium. *Physical Review B* 49, 14251-14269.

Kresse, G. and Hafner, J. (1994b) Norm-conserving and ultrasoft pseudopotentials for first-row and transition elements. *Journal of Physics: Condensed Matter* 6, 8245-8257.

Lawrence, P.J., Parker, S.C. and Tasker, P.W. (1987) Computer simulation studies of perfect and defective surfaces of $Cr_2O_3$. *Advances in Ceramics* 23, 247.

Lide, D.R. *CRC Handbook of Chemistry and Physics*, CRC, Boca Raton, Florida (2000)

Lindan, P.J.D. and. Gillan, M.J. (1993) Shell-model molecular dynamics simulation of superionic conduction in $CaF_2$. *Journal of Physics: Condensed Matter* 5, 1019-1030.

Mackrodt, W.C. (1989) Atomistic simulation of the surfaces of oxides. *Journal of the Chemical Society Faraday Transactions II* 85, 541-554.

Mackrodt, W.C. and Stewart, R.F. (1979) Defect properties of ionic solids. 2. Point-defect energies based on modified electron-gas potentials. *Journal of Physics C: Solid State Physics* 12, 431-449.

Mackrodt, W.C., Davey, R.J., Black, S.N. and Docherty, R. (1987) The morphology of alpha-$Al_2O_3$ and alpha-$Fe_2O_3$ – The importance of surface relaxation. *Journal of Crystal Growth*, 80, 441-446.

Manassidis, I. and Gillan, M.J. (1994) Structure and energetics of alumina surfaces calculated from first principles. *Journal of the American Ceramic Society* 77, 335-338.

Masri, P. and Tasker, P.W. (1985) Surface phonons and surface reconstruction and calcium-doped magnesium oxide, *Surface Science* 149, 209-225.

Mijoule, C. and Bouteiller, Y. (1991) Density functional calculation of the vibrational stretching mode of CO coadsorbed with ammonia on palladium clusters. *Surface Science* 253, 375-385.

Mitchell, D.T., Lee, S.B., Trofin, L., Li, N.C., Nevanen, T.K., Söderlund, H. and Martin, C.R. (2002) Smart nanotubes for bioseparations and biocatalysis. *Journal of the American Chemical Society* 124, 11864-11865.

Mitchell, P.J. and Fincham, D. (1993) Shell-model simulations by adiabatic dynamics. *Journal of Physics: Condensed Matter* 5, 1013-1038.

Mkhonto, D. and de Leeuw, N.H. (2002) A computer modelling study of the effect of water on the surface structure and morphology of fluorapatite: introducing a $Ca_{10}(PO_4)_6F_2$ potential model. *Journal of Materials Chemistry* 12, 2633-2644.

Mkhonto, D., Ngoepe, P.E., Cooper T.G. and de Leeuw, N.H. (2006) A computer

modelling study of the interaction of organic adsorbates with fluorapatite surfaces. *Physics and Chemistry of Minerals* 33, 314-331.

Mora-Fonz, M.J., Catlow, C.R.A. and Lewis, D.W. (2005) Oligomerization and cyclization processes in the nucleation of microporous silicas. *Angewandte Chemie – International Edition* 44, 3082-3086.

Mott, N.F. and Littleton, M.J. (1989) Conduction in polar crystals. 1. Electrolytic conduction in solid salts (reprinted from vol. 34, pg 485, 1938) *Journal of the Chemical Society Faraday Transactions II* 85, 565-579.

Narten, A.H. and Levy, H.A. (1971) Liquid water – molecular correlation functions from X-ray diffraction. *Journal of Chemical Physics* 55, 2263.

Nishiyama, N., Tanaka, S., Egashira, Y., Oku, Y. and Ueyama, K. (2003) Vapor-phase synthesis of mesoporous silica thin films. *Chemistry of Materials* 15, 1006-1011.

Nosé, S. (1984) A unified formulation of the constant temperature molecular dynamics methods. *Journal of Chemical Physics* 81, 511-519.

Oliver, P.M., Parker, S.C. and Mackrodt, W.C. (1993) Computer simulations of the crystal morphology of NiO. *Modelling in Material Science and Engineering* 1, 755-760.

Ostroverkhov, V. Waychunas, G.A. and Shen, Y.R. (2004) Vibrational spectra of water at water/alpha quartz (0001) interface. *Chemical Physics Letters* 386, 144-148.

Ostroverkhov, V. Waychunas, G.A. and Shen, Y.R. (2005) New information on water interfacial structure revealed by phase-sensitive surface spectroscopy. *Physical Review Letters* 94, 046102.

Pacchioni, G., Ferrari, A.M. and Bagus, P.S. (1996) Cluster and band structure ab initio calculations on the adsorption of CO on acid sites of the $TiO_2$ (110) surface. *Surface Science* 350, 159-175.

Parker, S.C. (1983) Prediction of mineral crystal structures. *Solid State Ionics* 8, 179-186.

Payne, M.C., Stich, I., De Vita, A., Gillan, M.J. and Clarke, L.J. (1993) Dynamics of dissociate chemisorption $Cl_2$/Si (111) - 2x1. *Faraday Discussions* 96, 151-159.

Perdew, J.P., Chevary, J.A., Vosko, S.H., Jackson, K.A., Pederson, M.R., Singh, D.J. and Fiolhais, C. (1992) Atoms, molecules, solids and surfaces – Applications of the generalized gradient approximation for exchange and correlation. *Physical Review B* 46, 6671-6687.

Pugh, S. and Gillan, M.J. (1994) the energetics of $NH_3$ adsorption at the MgO (001) surface. *Surface Science* 320, 331-343.

Puls, M.P., Woo, C.H. and Norgett, M.J. (1977) Shell-model calculations of interaction energies between point-defects and dislocations in ionic crystals. *Philosophical Magazine* 36, 1457-1472.

Purton, J., Bullett, D.W., Oliver, P.M. and Parker, S.C. (1995) Electronic structure and atomistic simulations of the ideal and defective surfaces of rutile. *Surface Science* 336, 166-180.

Rabone, J.A.L. and de Leeuw, N.H. (2006) Interatomic potential models for natural apatite crystals: incorporating strontium and the lanthanides. *Journal of Computer Chemistry* 27, 253-266.

Ramberg, H. (1954) A theoretical approach to the thermal stabilities of hydrous

minerals. 1. General principles as revealed by studies of hydroxides and oxyacids. *Journal of Geology* 62, 388-398.

Rosa, L., El-Barbary, A.A. Heggie, M.I. and Briddon, P.R. (2005) Structural and thermodynamic properties of water related defects in alpha quartz. *Physics and Chemistry of Minerals* 32, 323-331.

Rustad, J.R., Wasserman, E., Felmy, A.R. and Wilke, C. (1998) Molecular dynamics study of proton binding to silica surfaces. *Journal of Colloids and Interface Science* 198, 119-129.

Sakaguchi, I., Yurimoto, H. and Sueno, S. (1992) Self-diffusion along dislocations in single crystal MgO. *Solid State Communications* 84, 889-893.

Sanders, M.J., Leslie, M. and Catlow, C.R.A. (1984) Interatomic potentials for $SiO_2$. *Chemical Communications* 1271-1273.

Schroer, P., Kruger, P. and Pollman, J. (1994) Self-consistent electronic structure calculations of the (1010) surfaces of wurtzite compounds ZnO and CdS. *Physical Review B* 49, 17092-17101.

Smith, W. and Forester, T.R. (1996) DL_POLY 2.0: A general-purpose parallel molecular dynamics simulation package. *Journal of Molecular Graphics* 14, 136-141.

Soper, A.K. and Phillips, M.G. (1986) A new determination of the structure of water at 25 degrees C. *Chemical Physics* 107, 47-60.

Stauffer, L., Mharchi, A., Saintenoy, S., Pirri, C., Wetzel, P., Bolmont, D. and Gewinner, G. (1995) Surface electronic and atomic structure of $ErSi_{1.7}$ on Si (111). *Physical Review B*, 52, 11932-11937.

Stich, I., De Vita, A., Payne, M.C., Gillan, M.J. and Clarke, L.J. (1994) Surface dissociation from 1$^{st}$ principles – dynamics and chemistry. *Physical Review B* 49, 8076-8085.

Stoneham, A.M. (1976) *Defects and their Structure in Non-metallic Solids*, edited by B. Henderson and A.E. Hughes, Plenum, New York.

Swanston, D.M., McLean, A.B., McIlroy, D.N., Heskett, D., Ludeke, R., Munekata, H., Prietsch, M. and DiNardo, N.J. (1994) Surface localized states on InAs (110). *Surface Science* 312, 361-368.

Tasker, P.W and Duffy, D.M. (1984) The structure and properties of the stepped surfaces of MgO and NiO, *Surface Science* 137, 91-102.

Tasker, P.W, Colbourn, E.A. and Mackrodt, W.C. (1985) Segregation of isovalent impurity cations at the surfaces of MgO and CaO. *Journal of the American Ceramic Society* 68, 74-80.

Tasker, P.W. (1979) Stability of ionic crystal surfaces. *Journal of Physics C: Solid State Physics* 12, 4977-4984.

Tasker, P.W. (1987) *U.K.A.E.A. Report AERE-R-9130*, United Kingdom Atomic Energy Authority, Harwell, UK.

Tauson, V.L., Abramovich, M.G., Akimov, V.V. and Scherbakov, V.A. (1993) Thermodynamics of real mineral crystals – Equilibrium crystal shape and phase size effect. *Geochimica Cosmochimica Acta* 57, 815-821.

Vanderbilt, D. (1990) Soft self-consistent pseudopotentials in a generalized eigenvalue formalism. *Physical Review B* 41, 7892-7895.

Verlet, L. (1967) Computer experiments on classical fluids. 1. Thermodynamical properties of lennard-Jones moleucules. *Physical Review* 159, 98.

Wang, H.M., Henderson, G.S. and Brenan, J.M. (2004) Measuring quartz solubility by in situ weight-loss determination using a hydrothermal diamond cell. *Geochimica et Cosmochimica Acta* 68, 5197-5204.

Watson, G.W., Kelsey, E.T., de Leeuw, N.H., Harris, D.J. and Parker, S.C. (1996) Atomistic simulation of dislocations, surfaces and interfaces in MgO, *Journal Chemical Society Faraday Transactions* 92, 433-438.

Woensdregt, C.F. (1992) Computation of surface energies in an electrostatic point-charge model. 2. Application to zircon ($ZrSiO_4$). *Physics and Chemistry of Minerals* 19, 52-69.

Wulff, G. (1901) Zur Frage der Geschwindigkeit des Wachstums und der Auflösung der Kristallflachen. *Zeitschrift für Kristallographie Kristallgeometrie* 39, 449.

Zach, M.P., Newberg, J.T., Sierra, L., Hemminger, J.C. and Penner, R.M. (2003) Chemical vapor deposition of silica micro- and nanoribbons using step-edge localized water. *Journal of Physical Chemistry B* 107, 5393-5397.

Zhang, H.-F., Wang, C.-M., Buck, E.C. and Wang, L.-S. (2003) Synthesis, characterization and manipulation of helical $SiO_2$ nanosprings. *Nano Letters* 3, 577-580.